Journal of Power Sources 195 (2010) 7115–7119

Contents lists available at ScienceDirect

Journal of Power Sources

journal homepage: www.elsevier.com/locate/jpowsour

Short communication

Effect and function mechanism of amorphous sulfur on the electrochemical properties of cobalt hydroxide electrode

Dawei Song, Yijing Wang*, Qinghong Wang, Yaping Wang, Lifang Jiao, Huatang Yuan

Institute of New Energy Material Chemistry, Key Laboratory of Advanced Energy Materials Chemistry (Ministry of Education), Nankai University, Tianjin 300071, PR China

ARTICLE INFO

Article history:
Received 2 February 2010
Received in revised form 23 April 2010
Accepted 30 April 2010
Available online 7 May 2010

Keywords:
Negative electrode
Cobalt hydroxide
Amorphous sulfur
Function mechanism
Faradaic redox
Alkaline rechargeable battery

ABSTRACT

S-$Co(OH)_2$ composite is prepared via a facile co-precipitation method and investigated as negative electrode of Ni/Co battery. The addition of amorphous S improves the electrochemical properties of $Co(OH)_2$ electrode. The discharge capacity of S-$Co(OH)_2$ electrode can reach 413.2 mAh g^{-1} and still keep about 340 mAh g^{-1} after 300 cycles, which is much higher than that of S-free $Co(OH)_2$ electrode. Amorphous S in S-$Co(OH)_2$ electrode shows two functions during the charge–discharge process. One is that the addition of amorphous S with high specific surface area improves the dispersion of $Co(OH)_2$ platelets. The other is that the dissolution of amorphous S in electrode brings the new interspaces among the $Co(OH)_2$ platelets, these two factors largely increase the interspaces among $Co(OH)_2$ platelets. More interspaces are correlated to larger contact area with alkaline solution, which is in favor of the surface electrochemical redox. Thus, the capacity utilization of $Co(OH)_2$ is enhanced.

1. Introduction

Alkaline rechargeable nickel-based batteries employ nickel oxide electrodes as the positive electrodes [1], including nickel/cadmium (Ni/Cd), nickel/iron (Ni/Fe), nickel/zinc (Ni/Zn) and nickel/metal hydride (Ni/MH) batteries [2–12]. Among these batteries, Ni/Cd and Ni/MH batteries have been used widely. For the high energy and power density with low cost, Ni/Cd batteries were applied in many areas in a very long time, however, they have been replaced because cadmium is an awful poison that can contaminate the environment. Ni/MH batteries using hydrogen storage alloys as the negative electrode material have been drawing increasing attention due to their higher energy density both in terms of weight and volume, but the practical discharge capacity of commercial Ni/MH batteries is only about 330 mA h g^{-1}. In recent years, to meet the ever increasing needs for spacecrafts, defense, communication, electric vehicles, computers, camcorders, cellular phones, power tools and other home appliances, there was continuous demand to develop high power density and rechargeable batteries. Recently, a new type of Ni/Co battery using cobalt hydroxide as negative electrode is reported to have high discharge capacity and excellent cycle life. The reaction on cobalt hydroxide negative electrode is the Faradaic reaction between β-$Co(OH)_2$ and metallic Co during the charge–discharge process [13], and the same reversible transform is also observed on metallic Co negative electrode [14].

It is reported that some metalloids (such as Si, S, B, P, BN, Si_3N_4) can obviously improve the discharge capacity and cycle stability of metallic Co after mixing [15–20]. In addition, based on our recent experiments, Se and CNTs have the same effect on metallic Co. However, there are many disputes about the function mechanism of these metalloids on metallic Co electrode. Among these metalloids, sulfur is remarkable for its low cost and green environmental protection.

In this paper, in order to improve the discharge capacity and cycle life of cobalt hydroxide electrode, amorphous sulfur is added into cobalt hydroxide via a facile co-precipitation method, and the function mechanism of amorphous S on $Co(OH)_2$ electrode is investigated.

2. Experimental

2.1. Sample preparation

S-$Co(OH)_2$ is prepared via a facile co-precipitation method. In a typical procedure, 1 g $CoCl_2 \cdot 6H_2O$ and 1.04 g $Na_2S_2O_3 \cdot 5H_2O$ are dissolved in 20 ml deionized water under stirring. Then, 20 ml 80% $N_2H_4 \cdot H_2O$ and 1 g NaOH are added, repectively. After that, the precursor solution is transferred into a 50 ml Teflon-lined stainless steel autoclave and heated at 50 °C for 2 h. The final black precipitation is filted, washed and dried in vacuum for 12 h. The sample

* Corresponding author. Tel.: +86 22 23503639; fax: +86 22 23503639.
E-mail address: wangyj@nankai.edu.cn (Y. Wang).

0378-7753/$ – see front matter © 2010 Elsevier B.V. All rights reserved.
doi:10.1016/j.jpowsour.2010.04.088

obtained in this method is labeled as sample (a) for convenience. For comparison, S-free $Co(OH)_2$ is prepared by mixing 1 g $CoCl_2{\cdot}6H_2O$ and 1 g NaOH in 20 ml deionized water at 50 °C, and labeled as sample (b).

2.2. Structural and morphological characterization

The crystal structure and surface configuration of the samples are characterized by X-ray diffraction (XRD, Rigaku D/Max-2500, Cu Kα radiation), scanning electron microscopy (SEM, JEOL JSM-6700F Field Emission), energy dispersive X-ray spectrum (EDS, Kevex Sigma TM Quasar). Specific surface area is measured by BET method using a ST-08A specific surface area analyzer. The elemental composition is measured by inductive coupled plasma atomic emission spectroscopy (ICP-AES) on a USA Themo Jarrel-Ash Corp.

2.3. Electrochemical measurements

Negative electrodes are constructed through mixing as-prepared samples with carbonyl nickel powders at a weight ratio of 1:3. The powder mixture is pressed under 30 MPa pressure into a small pellet of 10 mm in diameter and 1.5 mm thickness. Electrochemical measurements are conducted in a three compartment cell using a Land battery test instrument (CT2001A). $NiOOH/Ni(OH)_2$ and Hg/HgO are used as the counter electrode and the reference electrode, respectively. The electrolyte solution is a 6 M KOH aqueous solution. The electrodes are charged at 200 mA g^{-1} for 3 h, discharged at 200 mA g^{-1} to −0.5 V (vs. Hg/HgO), the interval between charge and discharge is 5 min. Zahner IM6e electrochemical workstation is used for cyclic voltammetry (scan rate: 0.2 mV s^{-1}; potential interval: −1.2 to −0.2 V vs. Hg/HgO). All the tests are performed at room temperature.

3. Results and discussions

3.1. Material characterization

Fig. 1 shows the XRD patterns of sample (a) and sample (b). All sharp diffraction peaks in sample (a) and sample (b) can be indexed to the hexagonal cell of brucitelike β-$Co(OH)_2$ (space group $P\bar{3}m1$, JCPDS card, No. 74-1057). The sharp diffraction peaks suggest highly crystalline nature of sample (a) and sample (b). Moreover, no metallic Co peaks in sample (a) are detected, indicating no $CoCl_2{\cdot}6H_2O$ is reduced by $N_2H_4{\cdot}H_2O$. The weak broad peak located at $2\theta = 9°$ in sample (a) can be indexed to amorphous S (space group P21, JCPDS card, No. 74-2106), which is prepared via the redox reaction between $Na_2S_2O_3{\cdot}5H_2O$ and $N_2H_4{\cdot}H_2O$.

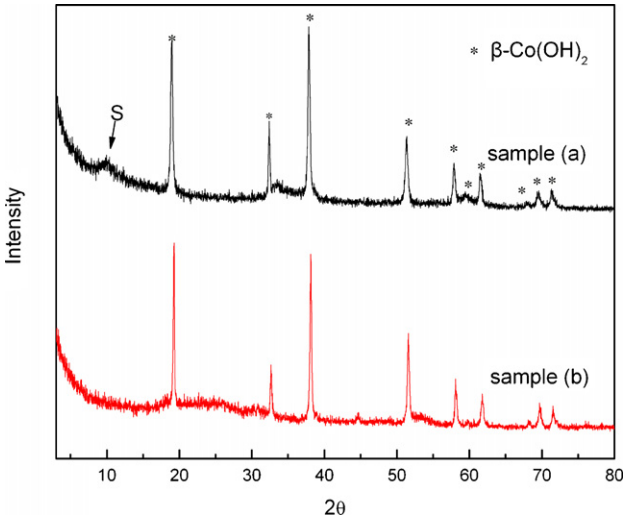

Fig. 1. XRD patterns of sample (a) and sample (b).

EDS results (Fig. 2) further confirm the presence of S in sample (a). Furthermore, the content of S is found to be 12.58 wt.%. In addition, the atomic ratio of Co:O is approximately about 1:2, which is consistent with the composition of $Co(OH)_2$.

Typical SEM images of sample (a) and sample (b) are illustrated in Fig. 3. It shows that there are some hexagonal platelets with irregular floccules distributing on the surface in sample (a), and there are only hexagonal platelets without irregular floccules in sample (b). From EDS measurement, the irregular floccules in sample (a) are amorphous S, and the hexagonal platelets in sample (a) and sample (b) are β-$Co(OH)_2$, which is consistent with the previous report [21]. Specific surface area is measured by BET method. The specific surface areas of sample (a) and sample (b) are 60.93 and 43.16 $m^2\ g^{-1}$, respectively. The higher specific surface areas of sample (a) should be attributed to amorphous S. The distributing of amorphous S with high specific surface area on $Co(OH)_2$ platelets improves the dispersion of $Co(OH)_2$ platelets and increases the interspaces among the $Co(OH)_2$ platelets.

3.2. Effect of amorphous S on electrochemical properties of $Co(OH)_2$ electrode

To investigate the structure change in charge–discharge process, XRD patterns of S-free $Co(OH)_2$ electrode at different cycles are compared in Fig. 4. It can be found that the diffraction peaks of

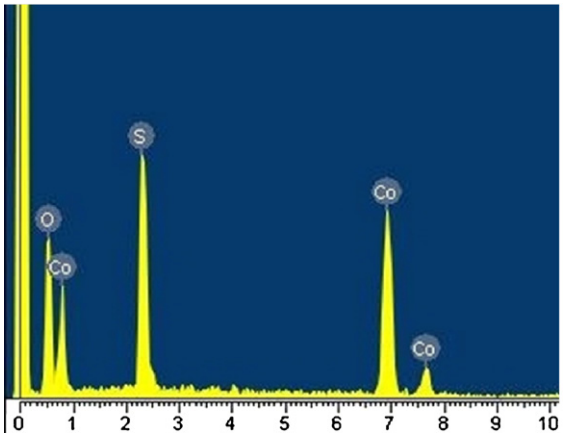

element	wt.%	atom%
O	31.97	59.98
S	12.58	11.77
Co	55.45	28.24
total	100.00	99.99

Fig. 2. EDS patterns and the related element composition of sample (a).

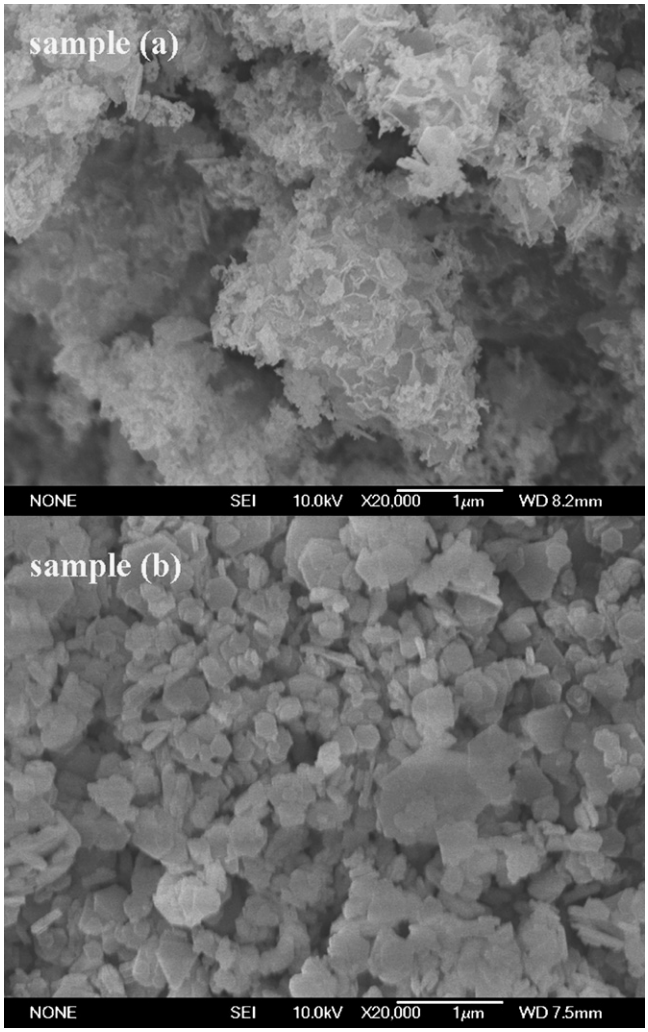

Fig. 3. SEM images of sample (a) and sample (b).

metallic Co are detected at the discharged state of the 1st cycle. At the charged state of the 2nd cycle, the peaks of β-$Co(OH)_2$ become weaker, while those of Co become stronger, illustrating that some $Co(OH)_2$ transforms into Co. On the contrary, the fully

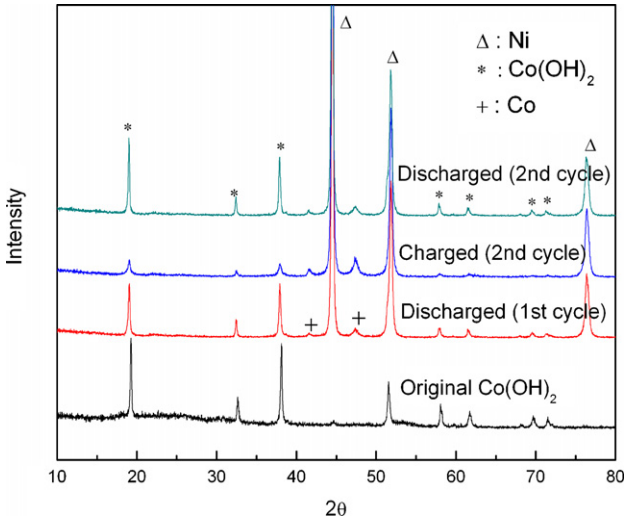

Fig. 4. XRD patterns of S-free $Co(OH)_2$ electrode at different cycles.

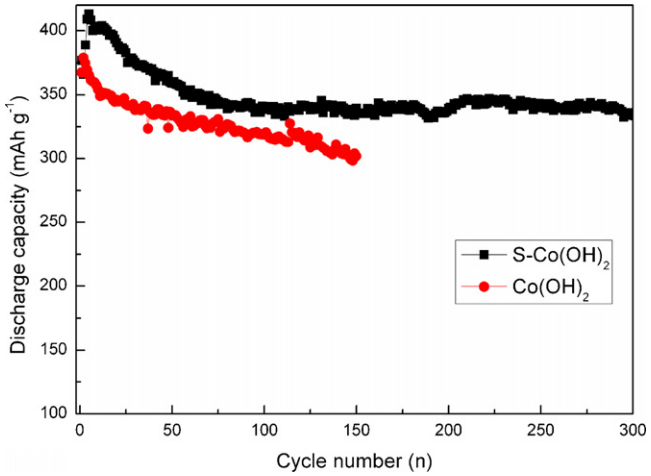

Fig. 5. Cycle life of S-free $Co(OH)_2$ and S-$Co(OH)_2$ electrodes (a).

discharged state of the 2nd cycle reveals a transformation from Co to β-$Co(OH)_2$. This means that β-$Co(OH)_2$ can be reduced to metallic Co during the charge process, and metallic Co can be oxidated to β-$Co(OH)_2$ during the discharge process. The discharge capacity of the electrode is mainly attributed to the electrochemical oxidation of metallic Co. Therefore, the charge–discharge reaction of $Co(OH)_2$ electrode can be expressed as:

$$Co(OH)_2 + 2e \underset{\text{discharge}}{\overset{\text{charge}}{\rightleftharpoons}} Co + 2OH^- \quad (1)$$

According to the above reversible electrochemical reaction, two electrons are transferred in the charge–discharge process. Based on Faraday's law, the theoretical electrochemical capacity of S-free $Co(OH)_2$ is 576 mAh g^{-1}.

Fig. 5 shows the cycle life of S-free $Co(OH)_2$ and S-$Co(OH)_2$ electrodes. At a current density of 200 mA g^{-1}, the discharge capacity of S-free $Co(OH)_2$ electrode reaches the maximum of 378.8 mAh g^{-1} at the second cycle and decreases gradually in the following charge–discharge cycles. After 150 charge–discharge cycles, the reversible discharge capacity still maintains about 301.8 mAh g^{-1}. It is noted that S-$Co(OH)_2$ electrode has an activation process and shows a higher discharge capacity and a better cycle performance, as compared to the S-free $Co(OH)_2$ electrode. At a current density of 200 mA g^{-1}, the discharge capacity of S-$Co(OH)_2$ electrode reaches the maximum of 413.2 mAh g^{-1} at the fifth cycle and decreases gradually in the initial 75 charge–discharge cycles. But after 75 cycles the discharge capacity begins to keep stable and the reversible discharge capacity still maintains about 340 mAh g^{-1} after 300 charge–discharge cycles, which is much higher than that of S-free $Co(OH)_2$ electrode and even higher than commercial AB_5 hydrogen storage alloys. The discharge capacity of amorphous S is near zero, so the improved discharge capacity cannot be attributed to amorphous S, but to the improved capacity utilization of $Co(OH)_2$ in the presence of amorphous S.

The charge–discharge curves of S-free $Co(OH)_2$ electrode and S-$Co(OH)_2$ electrode at the seventh cycle are shown in Fig. 6. The charge curves of the two samples both display two plateaus, charge plateaus and overcharge plateaus. It is obvious that S-$Co(OH)_2$ electrode displays higher charge plateaus and lower overcharge plateau as compared to S-free $Co(OH)_2$ electrode, indicating the addition of S increases the charge potential and decreases the overcharge potential of $Co(OH)_2$. Both two discharge plateaus appear at −0.75 to −0.77 V, lower than that of commercial hydrogen storage alloy (−0.90 V). It is noted that the length of charge plateaus and discharge plateaus in two electrodes is nearly same, showing both of the two electrodes have high coulombs efficiency and excellent

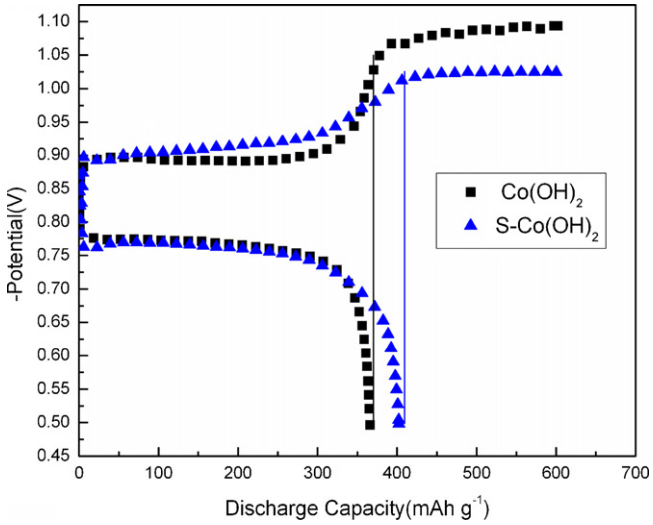

Fig. 6. Charge–discharge curves of S-free $Co(OH)_2$ electrode and S-$Co(OH)_2$ electrode.

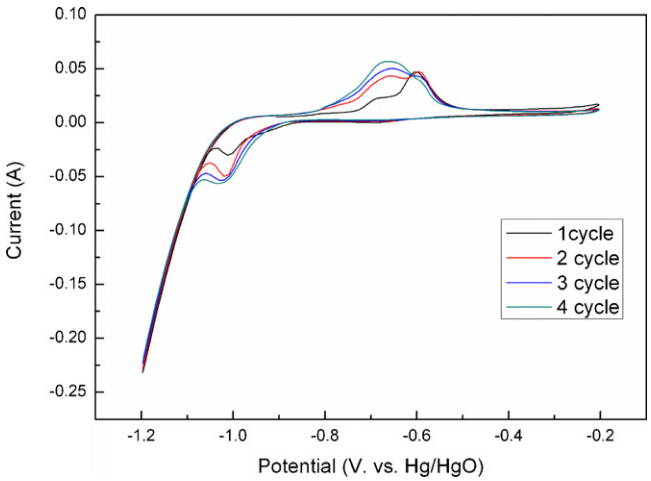

Fig. 7. CV curves of S-$Co(OH)_2$ electrode in the initial 4 cycles at a scan rate of 2 mV s^{-1}.

reversibility. From the charge–discharge curves, it can be concluded that the effect of amorphous S on $Co(OH)_2$ electrode is irreversible and only exists in the charge process.

To further confirm the electrochemical reaction process of the S-$Co(OH)_2$ electrode, cyclic voltammetry (CV) of S-$Co(OH)_2$ electrode during the initial four cycles at a scan rate of 2 mV s^{-1} is presented in Fig. 7. A pair of obvious redox peaks is detected, indicating that the reversible capacity is mainly based on the Faradaic redox mechanism. The curve shape and peak voltage in the fourth CV cycle are very similar to those of metallic Co powder electrode, confirming that there occurs the same reversible reaction on $Co(OH)_2$ electrode and metallic Co electrode. Based on the XRD patterns after charge and discharge (Fig. 4), the reduction peak is due to the reduction of β-$Co(OH)_2$ to metallic Co while the oxidation peak should be attributed to the oxidation of metallic Co to β-$Co(OH)_2$.

In the meantime, there is an activation process in the CV curves of S-$Co(OH)_2$ electrode during the initial four cycles, the integral area of the redox peaks increases gradually and peak voltage of the redox peaks shifts left gradually. In the first CV cycle, the oxidation peak and reduction peak appear around at the potential of −0.606 V and −1.012 (vs. HgO/Hg), respectively. The two potential is both higher than the oxidation potential and reduction potential of β-$Co(OH)_2$. In the third and fourth CV cycles, the oxidation peak and reduction peak shift slightly to −0.65 to −0.66 V and −1.03 to −1.04 V, and still higher than those of β-$Co(OH)_2$. In addition, the shift of the redox peaks is not observed in the CV curves of S-free $Co(OH)_2$ electrode during the initial four cycles. So except for the Faradaic redox reaction of β-$Co(OH)_2$, there is other reaction occurred in S-$Co(OH)_2$ electrode during four cycles. In order to investigate this reaction, the S elemental content in KOH aqueous solution and in S-$Co(OH)_2$ electrode is measured by ICP, S element is discovered in KOH aqueous solution after the first CV cycle and increases gradually during four cycles, and S element content in S-$Co(OH)_2$ electrode decreases gradually during four CV cycles, indicating amorphous S in S-$Co(OH)_2$ electrode is gradually dissolved into KOH aqueous solution during four CV cycles. So the left shift of the redox peaks should be attributed to the electrochemical dissolution of amorphous S.

3.3. Function mechanism of amorphous S on $Co(OH)_2$ electrode

Based on our experiments, the function mechanism of amorphous S on $Co(OH)_2$ electrode can be described as Scheme 1.

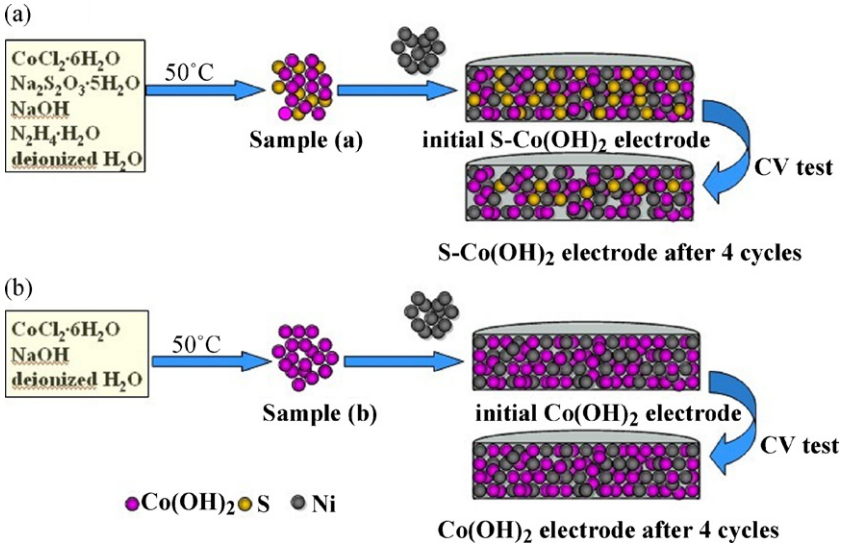

Scheme 1. The function schematic representation of amorphous S on $Co(OH)_2$ electrode.

Compared to S-free $Co(OH)_2$ electrode, amorphous S in S-$Co(OH)_2$ electrode shows two functions during the charge–discharge process. One is that the addition of amorphous S with high specific surface area improves the dispersion of $Co(OH)_2$ platelets. The other is that the dissolution of amorphous S in electrode brings new interspaces among the $Co(OH)_2$ platelets, these two factors largely increase the interspaces among the $Co(OH)_2$ platelets. As we know, more interspaces are correlated to larger contact area with alkaline solution, which is in favor of the surface electrochemical redox. Thus, the capacity utilization of $Co(OH)_2$ is enhanced. But it is not that the more amorphous S is added, the higher discharge capacity can be obtained, because too much amorphous S added will bring much interspaces among $Co(OH)_2$ platelets, leading to poor electrical conductivity. The reaction on S-free $Co(OH)_2$ negative electrode is the Faradaic reaction between β-$Co(OH)_2$ and metallic Co during the charge–discharge process, so this mechanism can also be used to explain the function mechanism of some metalloids (such as Si, S, B, P, BN, Si_3N_4, Se, CNTs) on metallic Co electrode.

4. Conclusion

This paper investigates the effect and function mechanism of amorphous S on $Co(OH)_2$ electrode, and proves that the addition of amorphous S improves the electrochemical properties of $Co(OH)_2$ electrode. A proper function mechanism of amorphous S on $Co(OH)_2$ electrode is proposed for the first time. This mechanism can also be used to explain the function mechanism of some metalloids on metallic Co electrode. This discovery provides a new way to improve electrochemical properties of Co negative electrode and $Co(OH)_2$ negative electrode of alkaline rechargeable Ni-based batteries and a guidance for improving the electrochemical properties of other negative electrodes based on the Faradaic redox mechanism.

Acknowledgments

This work is financially supported by MOST program (2007AA05Z149, 2007AA05Z108, 2010CB631303), NSFC (50631020, 50701025, 50971071).

References

[1] A.K. Shukla, S. Venugopalan, B. Hariprakash, J. Power Sources 100 (2001) 125–148.
[2] K. Vijayamohanan, T.S. Balasubramanian, A.K. Shukla, J. Power Sources 34 (1991) 269–285.
[3] K. Micka, Z. Zabransky, J. Power Sources 19 (1987) 315–323.
[4] M.E. Unates, E. Folquer, J.R. Vilche, A.J. Arvia, J. Electrochem. Soc. 139 (1992) 2697–2704.
[5] E.J. Casey, A.R. Dubois, P.E. Lake, W.J. Moroz, J. Electrochem. Soc. 112 (1965) 371–383.
[6] X.Y. Xiong, H. Vander Poorten, M. Crappe, Electrochim. Acta 41 (1996) 1267–1275.
[7] A. Yuan, J. Zhao, Electrochim. Acta 51 (2006) 2454–2462.
[8] W.B. Gu, C.Y. Wang, S.M. Li, M.M. Geng, B.Y. Liaw, Electrochim. Acta 44 (1999) 4525–4541.
[9] S.R. Ovshinsky, M.A. Fetcenko, J. Ross, Science 260 (1993) 176–181.
[10] W. Yin, M. Zhao, Electrochim. Acta 52 (2007) 2723–2728.
[11] J. Jindra, J. Power Sources 66 (1997) 15–25.
[12] Y.F. Yuan, J.P. Tu, H.M. Wu, Y.Z. Yang, D.Q. Shi, X.B. Zhao, Electrochim. Acta 51 (2006) 3632–3636.
[13] X.P. Gao, S.M. Yao, T.Y. Yan, Z. Zhou, Energy Environ. Sci. 2 (2009) 502–505.
[14] A. Durairajan, B.S. Haran, B.N. Popov, R.E. White, J. Power Sources 83 (1999) 114–120.
[15] G. He, L.F. Jiao, H.T. Yuan, Y.Y. Zhang, Y.J. Wang, Electrochem. Commun. 8 (2006) 1633–1638.
[16] Q.H. Wang, L.F. Jiao, H.M. Du, W.X. Peng, S.C. Liu, Y.J. Wang, et al., Int. J. Hydrogen Energy (2010), doi:10.1016/j.ijhydene.2009.12.002.
[17] D.W. Song, Y.J. Wang, Y.P. Wang, L.F. Jiao, H.T. Yuan, Electrochem. Commun. 10 (2008) 1486–1489.
[18] Y.L. Cao, W.C. Zhou, X.Y. Li, X.P. Ai, X.P. Gao, H.X. Yang, Electrochim. Acta 51 (2006) 4285–4290.
[19] Z.W. Lu, S.M. Yao, G.R. Li, T.Y. Yan, X.P. Gao, Electrochim. Acta 53 (2008) 2369–2375.
[20] S.M. Yao, K. Xi, G.R. Li, X.P. Gao, J. Power Sources 184 (2008) 657–662.
[21] Z.P. Liu, R.Z. Ma, Mi. Osada, K. Takada, T. Sasaki, J. Am. Chem. Soc. 127 (2005) 13869–13874.